Since January 2020 Elsevier has created a COVID-19 resource centre with free information in English and Mandarin on the novel coronavirus COVID-19. The COVID-19 resource centre is hosted on Elsevier Connect, the company's public news and information website.

Complement associated microvascular injury and thrombosis in the pathogenesis of severe COVID-19 infection: A report of five cases

Cynthia Magro , J. Justin Mulvey , David Berlin , Gerard Nuovo , Steven Salvatore , Joanna Harp , Amelia Baxter-Stoltzfus , Jeffrey Laurence

PII: S1931-5244(20)30070-0
DOI: https://doi.org/10.1016/j.trsl.2020.04.007
Reference: TRSL 1415

To appear in: *Translational Research*

Received date: 9 April 2020
Accepted date: 9 April 2020

Please cite this article as: Cynthia Magro , J. Justin Mulvey , David Berlin , Gerard Nuovo , Steven Salvatore , Joanna Harp , Amelia Baxter-Stoltzfus , Jeffrey Laurence , Complement associated microvascular injury and thrombosis in the pathogenesis of severe COVID-19 infection: A report of five cases, *Translational Research* (2020), doi: https://doi.org/10.1016/j.trsl.2020.04.007

Complement associated microvascular injury and thrombosis in the pathogenesis of severe COVID-19 infection: A report of five cases

Cynthia Magro,[1] J. Justin Mulvey,[2] David Berlin[3], Gerard Nuovo[4] Steven Salvatore[1], Joanna Harp[5], Amelia Baxter-Stoltzfus,[1] and Jeffrey Laurence[6]

From: [1]Department of Pathology and Laboratory Medicine, Weill Cornell Medicine; [2]Department of Laboratory Medicine, Memorial Sloan-Kettering Cancer Center; and [3]Department of Medicine, Division of Pulmonary and Critical Care Medicine, Weill Cornell Medicine, New York, NY, USA [4]The Ohio State University Comprehensive Cancer Center, Columbus Ohio and Discovery Life Sciences, Powell, Ohio; [5]Department of Dermatology, Weill Cornell Medicine; and [6]Department of Medicine, Division of Hematology and Medical Oncology, Weill Cornell Medicine, New York, NY, USA.

Correspondence to: Jeffrey Laurence, MD, Weill Cornell Medicine, 1300 York Avenue, New York, NY 10065. E-mail: jlaurenc@med.cornell.edu.

At a Glance Commentary

Background

The respiratory distress syndrome accompanying a subset of severe COVID-19 may be distinct from classic ARDS. There is relatively well-preserved lung mechanics despite the severity of hypoxemia, characterized by high respiratory compliance and high shunt fraction, and increasing recognition of systemic features of a hypercoaguable state in this disease. Therefore, the pathology and pathophysiology of COVID-19 might differ from that of typical ARDS. We sought to define the role of complement activation and microvascular thrombosis in cases of persistent, severe COVID-19.

Translational Significance

A pattern of tissue damage consistent with complement-mediated microvascular injury was noted in the lung and/or skin of five individuals with severe COVID-19. Our demonstration of the striking deposition of C5b-9, C4d, and MASP2 in the microvasculature of two organ systems is consistent with profound and generalized activation of both alternative and lectin-based pathways. It provides a foundation for further exploration of the pathophysiologic importance of complement in COVID-19, and could suggest targets for specific intervention.

Abstract

Acute respiratory failure and a systemic coagulopathy are critical aspects of the morbidity and mortality characterizing infection with severe acute respiratory distress syndrome-associated coronavirus-2 (SARS-CoV-2), the etiologic agent of Coronavirus disease 2019 (COVID-19). We examined skin and lung tissues from 5 patients with severe COVID-19 characterized by respiratory failure (n=5) and purpuric skin rash (n=3). The pattern of COVID-19 pneumonitis was predominantly a pauci-inflammatory septal capillary injury with significant septal capillary mural and luminal fibrin deposition and permeation of the inter-alveolar septa by neutrophils. No viral cytopathic changes were observed and the diffuse alveolar damage (DAD) with hyaline membranes, inflammation, and type II pneumocyte hyperplasia, hallmarks of classic ARDS, were not prominent. These pulmonary findings were accompanied by significant deposits of terminal complement components C5b-9 (membrane attack complex), C4d, and mannose binding lectin (MBL)-associated serine protease (MASP)2, in the microvasculature, consistent with sustained, systemic activation of the alternative and lectin-based complement pathways. The purpuric skin lesions similarly showed a pauci-inflammatory thrombogenic vasculopathy, with deposition of C5b-9 and C4d in both grossly involved and normally-appearing skin. In addition, there was co-localization of COVID-19 spike glycoproteins with C4d and C5b-9 in the inter-alveolar septa and the cutaneous microvasculature of two cases examined. In conclusion, at least a subset of sustained, severe COVID-19 may define a type of catastrophic microvascular injury syndrome mediated by activation of complement pathways and an associated procoagulant state. It provides a foundation for further exploration of the pathophysiologic importance of complement in COVID-19, and could suggest targets for specific intervention.

Introduction

The severe acute respiratory distress syndrome-associated coronavirus-2 (SARS-CoV-2), etiologic agent of Coronavirus disease 2019 (COVID-19), was initially identified in Wuhan, Hubei, China in December 2019 (1). It was documented to be pandemic by the World Health Organization in early March 2020 (2), and by early April there were over 1.5 million cases worldwide, with over 90,000 deaths (3). Organ dysfunction, particularly progressive respiratory failure and a generalized coagulopathy, are associated with the highest mortality (1,4,5).

It was soon recognized that SARS-CoV-2 is but one of a large pool of pre-pandemic SARS-like bat coronaviruses which replicate in primary human airway epithelial cells, using human Angiotensin Converting Enzyme (ACE)2 entry receptors (6). These include the etiologic agents of the original SARS-CoV and Middle East respiratory syndrome (MERS)-CoV, for which mortality is also linked to severe respiratory failure, with pathologic evidence of ARDS (7). Preliminary pathology studies of COVID-19 patients demonstrated diffuse alveolar damage (DAD) with edema, hyaline membranes, and inflammation, followed by type II pneumocyte hyperplasia, features characteristic of typical ARDS (8,9). But many patients with COVID-19-related severe respiratory distress have a delayed onset of respiratory distress (10), then manifest relatively well-preserved lung mechanics, despite the severity of hypoxemia, characterized by high respiratory compliance and high shunt fraction, and prolonged requirement for mechanical ventilation (10,11). Therefore, significant aspects of the pathology of COVID-19 might be expected to differ from classic ARDS.

We examined lung and cutaneous tissues from 5 patients with SARS-CoV-2 infection and severe respiratory failure, 3 of whom also had features consistent with a systemic procoagulant state, including retiform purpura or livedo racemosa—prominent dermatologic signs of a generalized microvascular thrombotic disorder—and markedly elevated d-dimers. Histologic and immunohistochemistry studies defined a pattern of cutaneous and pulmonary pathology involving microvascular injury and thrombosis, consistent with activation of the alternative pathway (AP) and lectin pathway (LP) of complement. Co-localization of SARS-CoV-2-specific spike glycoproteins with complement components in the lung and skin was also documented. Our studies suggest that at least a subset of severe COVID-19 infection involves a catastrophic, complement-mediated thrombotic microvascular injury syndrome with sustained activation of the AP and LP cascades. Potential mechanisms of complement activation, including

involvement of positive feedback loops with the coagulation system, are discussed in the context of hypothesis-generating studies providing the foundation for potential therapeutic intervention.

Methods

Patient population: All five patients were selected for pathologic studies based on a respiratory tract sample positive for SARS-CoV-2 in a reverse transcriptase-polymerase chain reaction assay, as tested by a designated diagnostic laboratory. They represent the first two patients succumbing to COVID-19 and undergoing autopsy that were available to us, and the first three infected individuals for whom a dermatologic consult had been requested to evaluate an extensive skin rash. These five cases were assembled over a period of two weeks. A respiratory pathogen PCR panel was used to test for other potential pulmonary viral pathogens, along with standard bacterial and fungal respiratory cultures, and these tests were unrevealing. Cases 2, 3 and 4 received hydroxychloroquine and/or azithromycin, as noted, with dosing as: hydroxychloroquine, 600mg every 12 hours for one day then 400mg every 12 hours for 4 days; azithromycin: 500mg daily for 5 days .

Microscopic and immunohistologic studies: Routine light microscopy and immunohistochemical (IHC) assessment for the deposition of C5b-9 (membrane attack complex, MAC), C3d, and C4d via a diaminobenzidene (DAB) technique was conducted. Identification of C5b-9, C3d, or C4d within any epithelial basement membrane zone, elastic fibers, or the elastic lamina of vessels was considered nonspecific staining. IHC was performed using C3d (Cell Marque, Rocklin CA, 403A-78), C4d (Alpco, Salem NH, BI-RC4d), C5b-9 (Agilent, Santa Clara CA, M077701-5), and MASP2 (Sigma, St. Louis, MO, HPA029313) antibodies on paraffin embedded sections using a modified Leica protocol. Heat mediated antigen retrieval with Tris-EDTA buffer (pH = 9, epitope retrieval solution 2) was performed for 20 min, followed by incubation with each antibody for 15 min. Details have been described by one of the authors, including documentation of the involvement of many of these complement components in pathologic processes linked to complement activation in both dermal and lung tissues (12-15). Staining for SARS-CoV-2 spike (catalogue #3525) and envelope (catalogue #3531) proteins (Prosci, Poway, CA) was optimized with cells from nasopharyngeal preparations obtained from individuals known to be positive or negative for the virus before being employed in the current studies. It involves use of horseradish peroxidase conjugate (ENZO, catalogue #ADI-950-113-

0100) and an HRP-conjugated compact polymer system, with DAB as chromogen. Hematoxylin and eosin counterstain was used and mounted with Leica Micromount.

Results

Case 1. A 62 year-old male with a history of coronary artery disease, diabetes mellitus, heart failure with preserved ejection fraction, prior treatment for hepatitis C virus infection, and end-stage renal disease on intermittent hemodialysis was evaluated in an emergency department (ED), in extremis and obtunded. He had severe hypoxemia and a blood pressure of 180/100. His international normalized ratio (INR) was mildly elevated at 1.2, with a partial thromboplastic time (PTT) within the normal range (23.0-37.0), and normal platelet count (178 x 10^9/L). Chest x-ray demonstrated bilateral airspace opacities most prominent in the peri-hilar distribution. After discussion with his family, he was placed on comfort measures and died a few hours after presentation. A limited autopsy was performed. Grossly, the lungs had a congested and hemorrhagic appearance. Light microscopic examination revealed a severe organizing hemorrhagic pneumonitis (Fig. 1A), including significant fibrin deposition within septal capillary lumens and walls accompanied by endothelial cell necrosis, consistent with a thrombotic necrotizing capillary injury syndrome (Fig. 1B). The pattern of septal capillary injury ranged from a pauci-inflammatory pattern (Fig. 1C) to one characterized by permeation of the inter-alveolar septa by neutrophils amidst the damaged capillaries, along with intra-alveolar neutrophils (Fig. 1D). No viral cytopathic changes were observed. Hyaline membranes reflective of DAD were not observed. In addition, and in contrast to preliminary reports of COVID-19 lung pathology (8,9), type II pneumocyte hyperplasia was not appreciated (Fig. 1A-D). The brunt of the lung injury was restricted to septal capillaries, without pneumocyte involvement.

Extensive C4d deposition localized to the inter-alveolar septal capillaries was then demonstrated (Fig. 2A,B). C5b-9 deposition was also seen, showing a similar pattern of septal capillary localization as for C4d, although reduced in intensity (Fig. 2C). Granular deposition of C3d was also noted; although minimal in comparison to the C5b-9 and C4d deposits, it expressed a similar pattern of septal capillary localization (Fig. 2D). MASP2 staining was attempted but, due to high background staining in this case, was deemed technically unsatisfactory.

In order to explore possible generalized complement activation in this patient, a sample of clinically-appearing normal skin was also found to have significant vascular deposits of C5b-9 within dermal capillaries (not shown).

Case 2. A 73 year-old male with a history of smoking, obesity, and pre-diabetes developed respiratory distress and was evaluated in the ED. He was febrile, tachypneic, severely hypoxemic, and required emergent endotracheal intubation. He had a serum creatinine of 2.4. Chest x-ray showed bilateral airspace opacities. Sedatives and neuromuscular blockade were used to enforce a lung protective low-stretch strategy. His course was complicated by atrial fibrillation, shock, and progressive renal failure. His INR and PTT were within normal limits. On the 4th day of mechanical ventilation the patient developed thrombocytopenia (platelets 148 x 10^9/L) and severe hypercapnia, with a dramatic increase in the estimated pulmonary dead space fraction, and expired the following day. A limited autopsy demonstrated a pattern of lung injury that mirrored Case 1. Grossly, the lungs had a hemorrhagic and congested appearance. Microscopically, the lungs showed extensive hemorrhagic pneumonitis. The inter-alveolar septa were congested, with luminal and mural fibrin deposition within septal capillaries. Focal intra-alveolar collections of neutrophils and monocytes were seen. Viral cytopathic changes were not appreciated. Due to vascular compromise, there was concomitant striking red cell extravasation found within the alveolar spaces, along with intra-alveolar fibrin deposition. Unlike Case 1, there was some focal hyaline membrane formation and type II pneumocyte hyperplasia in areas of hemorrhagic pneumonitis (Fig. 3A-D). However, unlike Case 1, this patient had been on ventilator support for one week, which can itself lead to some DAD, and yet, as in Case 1, the dominant pattern was septal capillary injury, not DAD.

On IHC there was prominent deposition of C5b-9 within the microvasculature of the inter-alveolar septa as well as in larger caliber vessels of the lung parenchyma (Fig. 4A,B). Of interest, C5b-9 septal deposition was not limited to areas of diseased lung, but was also seen in normal-appearing lung and tracheal soft tissues, while C4d was localized to inter-alveolar septa in regions of microvascular injury (Fig. 4C,D). MASP2 staining demonstrated granular and punctate staining localized to the inter-alveolar septa (Fig. 4E).

Case 3. A 32 year-old male with a medical history of obesity-associated sleep apnea and anabolic steroid use, currently taking testosterone, presented with a 1 week history of fever and cough. He became progressively more dyspenic with fevers to 40°C, ultimately becoming ventilator dependent from acute respiratory failure. Chest x-ray showed bilateral airspace

opacities. He had an elevated d-dimer of 1024ng/ml (normal range 0-229) on presentation, which peaked at 2090ng/ml on hospital day 19, and a persistently elevated INR of 1.6-1.9, but a normal PTT and platelet count. Serum complement levels for CH50 (177 CAE Units, normal range 60-144), C4 (42.6 mg/dL, normal range 12-36), and C3 (178 mg/dL, normal range 90-180) were elevated. Over his continuing three-plus weeks on ventilator support he completed courses of hydroxychloroquine and azithromycin, followed by the experimental anti-CoV agent remdesivir (5mg/kg i.v. daily for 10 days).

After only 4 days on ventilator support, retiform purpura with extensive surrounding inflammation was noted on his buttocks (Fig. 5A). Skin biopsy showed a striking thrombogenic vasculopathy accompanied by extensive necrosis of the epidermis and adnexal structures, including the eccrine coil. There was a significant degree of interstitial and perivascular neutrophilia with prominent leukocytoclasia (Fig. 5B). IHC showed striking and extensive deposition of C5b-9 within the microvasculature (Fig. 5C).

Case 4. A 66 year-old female, with no significant past medical history, was brought to the ED after 9 days of fever, cough, diarrhea, and chest pain. She was hypoxemic, with diffuse bilateral patchy airspace opacities, without effusions, on chest x-ray. She was admitted and treated with hydroxychloroquine and prophylactic anticoagulation with enoxaparin. Three days later she became confused, increasingly hypoxemic with rising serum creatinines, and was intubated. Renal replacement was initiated. On hospital day 10, thrombocytopenia (platelets 128 x 10^9/L) and a markedly elevated d-dimer of 7030ng/ml, but normal INR and PTT, were noted. The next day dusky purpuric patches appeared on her palms and soles bilaterally (Fig. 6A). A skin biopsy of one lesion showed superficial vascular ectasia and an occlusive arterial thrombus within the deeper reticular dermis in the absence of inflammation (Fig. 6B). Extensive vascular deposits of C5b-9 (Fig. 6C), C3d, and C4d (Fig. 6D) were observed throughout the dermis, with marked deposition in an occluded artery. A biopsy of normal-appearing deltoid skin also showed conspicuous microvascular deposits of C5b-9 (Fig. 6E). Sedative infusions were discontinued that day, unmasking a comatose state. Computerized tomographic imaging of the head revealed multifocal supra- and infra-tentorial infarctions, with complete infarction of the area supplied by the left middle cerebral artery.

Case 5. A 40 year-old female, with no significant past medical history, presented to the ED after 2 weeks of dry cough, fever, myalgias, diarrhea, and progressive dyspnea. She had been diagnosed one week earlier, at an outside hospital, with COVID-19. Electrocardiogram revealed severely reduced left ventricular function. Patchy bilateral airspace opacities were noted and she was soon intubated for respiratory failure and shock. D-dimer was elevated at 1187ng/ml, with a normal platelet count and PTT, but an elevated INR of 1.4. Mildly purpuric reticulated eruptions on her chest, legs and arms, consistent with livedo racemosa, were noted (Fig. 7A), and a skin biopsy performed. There was a modest perivascular lymphocytic infiltrate in the superficial dermis along with deeper seated small thrombi within rare venules of the deep dermis, in the absence of a clear vasculitis (Fig. 7B). Significant vascular deposits of C5b-9 (Fig. 7C) and C4d (Fig. 7D) were observed. As for Case 4, a biopsy of normal deltoid skin showed microvascular deposits of C5b-9 throughout the dermis (Fig. 7E).

Co-localization of SARS-CoV-2 envelope proteins with complement components in dermal and pulmonary microvessels of two COVID-19 patients

SARS-CoV-2 spike and envelope proteins strongly localized to the respiratory epithelia and the inter-alveolar septa in tissue from Case 1. No signal was found in control lung samples (data not shown)**.** Using NUANCE software, by which the fluorescent signal tagging CoV proteins appears red and the DAB chromogen tagging C4d appears green, a merged image shows a strong yellow signal indicative of septal capillary C4d and SARS-CoV-2 co-localization (Fig. 8A-D). A similar analysis in which the DAB chromogen was used to tag C5b-9 also gave a merged image with a strong yellow signal, indicative of septal vascular C5b-9 co-deposition with SARS-CoV-2 protein (Fig. 8E-H). In terms of the skin, co-localization of C4d with SARS-CoV-2 glycoprotein was demonstrated for Case 2 (Fig. 9A,B).

Discussion

Using pulmonary and cutaneous biopsy and autopsy samples from five individuals with severe COVID-19 we document that at least some SARS-CoV-2-infected patients who become critically ill suffer a generalized thrombotic microvascular injury. Such pathology involves at least the lung and skin, and appears mediated by intense complement activation. Specifically, we found striking septal capillary injury accompanied by extensive deposits of the terminal

complement complex C5b-9 as well as C4d and MASP2 in the lungs of two cases examined, and a similar pattern of pauci-inflammatory complement mediated microthrombotic disease in the skin of three cases with retiform and purpuric lesions, with C5b-9 and C4d deposition in samples taken from both cutaneous lesions and normal-appearing skin.

Our histologic findings are consistent with emerging observations suggesting that COVID-19 has clinical features distinct from typical ARDS. That is, COVID-19-related severe respiratory distress can be manifest by relatively well-preserved lung mechanics, despite the severity of hypoxemia, characterized by high respiratory compliance, high shunt fraction, and prolonged requirement for mechanical ventilation (10,11). The pathology in these cases might therefore be expected to differ from the diffuse alveolar damage and hyaline membrane formation which are hallmarks of typical ARDS. Albeit preliminary pathology studies of lungs from COVID-19 cases described DAD with edema, hyaline membranes, and inflammation, followed by type II pneumocyte hyperplasia, features characteristic of typical ARDS (8,9), the pulmonary abnormalities in our patients appear largely restricted to the alveolar capillaries, i.e., more of a thrombotic microvascular injury with few signs of viral cytopathic or fibroproliferative changes. An increase in the dead space fraction might be anticipated with this type of pathology, i.e., respiratory failure accompanied by greater lung compliance and less pulmonary consolidation than is characteristic of typical ARDS. Indeed, the histologic pattern of pauci-cellular terminal lung parenchymal injury with septal capillary damage we document resembles images captured in early case reports in the Chinese language literature of severe COVID-19 pneumonitis (16).

We now show that this pathologic pattern, atypical for classic ARDS, is accompanied by extensive deposition of AP and LP complement components within the lung septal microvasculature. With such extensive complement involvement, membrane attack complex-mediated microvascular endothelial cell injury and subsequent activation of the clotting pathway, leading to fibrin deposition, might be anticipated (17), as observed in our cases. It is also consistent with the very high d-dimer levels found in the three cases in which it was assessed. Vascular deposition of C5b-9 is a key feature of many microthrombotic syndromes, regardless of the particular syndromic complex, including catastrophic antiphospholipid antibody syndrome, atypical hemolytic uremic syndrome, purpura fulminans and severe multi-organ malignant atrophic papulosis, and they may respond to anti-complement therapies (18-23).

A pre-clinical model of SARS infection emphasizes the potential role of complement in the parenchymal lung injury of coronavirus infection (7). Mouse-adapted SARS-CoV MA15 infection of $C3^{-/-}$ mice led to significantly less weight loss and respiratory dysfunction than seen in wild-type mice, and this occurred despite equivalent viral loads in the lung (7). Another feature reflective of a prominence of complement-mediated pathology rather than simply inflammation or vasculitis in our COVID-19 patients was the extent of septal and intra-alveolar neutrophilia. It was present, but pauci-inflammatory. SARS-CoV-infected wild-type mice also had higher levels of neutrophils in the lung than their $C3^{-/-}$ counterparts (7). Tissue neutrophilia may be attributable to the neutrophil chemoattractant properties of complement. Both neutrophils and complement are key sentinels of innate immunity and also modulate thrombogenic pathways, the latter thought related to C5a receptor/tissue factor cross-talk mediated by neutrophils (24). Neutrophilia in human SARS-CoV patients is associated with a poor outcome and could be an index of the extent of complement activation (7,25). Peripheral neutrophilia is not a significant observation in limited series of COVID-19 patients from China (26) or the U.AS. (27), although there are insufficient numbers to assess its correlation with severity of disease. We have observed an increase in peripheral blood neutrophil vacuolization and granule content in our patients, consistent with an activated state, even if absolute numbers are not elevated.

Systemic activation of complement was reflected by elevated complement levels in the sera of SARS-CoV-infected wild-type mice. We measured complement levels in only one of our cases, Case 3. They were only moderately elevated, perhaps reflecting consumption in tissues, with reciprocal depression of circulating levels. Indeed, we found deposition of AP and LP components in normal-appearing skin in 3 cases, not only in biopsies of retiform cutaneous lesions from those patients. Retiform purpura reflects the cutaneous manifestation of an occlusive microthrombotic process (28). In summary, while complement does not appear to play a major role in controlling CoV replication, it may have a critical role in its pathogenicity.

There are several intriguing questions that remain to be addressed as additional cases are investigated. For example, one might have anticipated thrombocytopenia in the context of a systemic microvascular thrombosis in our cases. Although mild thrombocytopenia (100-150 x 10^9/L) has been recorded in 20% of COVID-19 patients (26), such values were seen in only 2 of our 5 patients, nor were platelets a prominent component of the fibrin microthrombi seen

histologically. It is possible that infection-related thrombocytosis was mitigated by the development of severe vasculopathy. However, there is also precedent for such platelet values in an atypical hemolytic-uremic syndrome (aHUS)-type of microangiopathy. Platelet counts may be in the normal range despite severe thrombotic disease (29). Second, there appears to have been a delay of 5-9 days in most, if not all, of our patients between the onset of typical respiratory symptoms, including a non-productive cough, myalgias, fatigue, fever, and mild dyspnea, and a catastrophic change in respiratory status. This may reflect an evolution of immune processes—anti-viral IgM levels would expect to emerge at this point—or perhaps the fact that the complement cascade is a threshold pathway. When activated to a great extent it may exceed the capacity of complement regulatory proteins, both soluble and normally present in abundance on the microvasculature (29). That raises the issue of why only a subset of SARS-CoV2-infected patients develops such severe disease with features atypical for ARDS. The age range was wide among our cases, as was the degree of pre-existing immune suppression. But there are a variety of complement regulatory factor polymorphisms or mutations (21) as well as coagulation pathway mutations which could promote susceptibility to enhanced complement activation and thrombosis in a given individual that should be investigated.

Our results, particularly when viewed in the context of murine models of SARS-CoV infection, suggest the hypothesis that intervention with inhibitors of the alternative or lectin complement pathways, or both, may be relevant to severe COVID-19 in humans. Multiple studies have documented a role for the AP in microvascular injury (30), as characterized by C5b-9 deposition (13,31), but the lectin pathway has not been similarly investigated. Support for the involvement of the LP in COVID-19 comes from the discovery that MBL binds to the SARS-CoV spike glycoprotein (32). A complex of MBL with MASP-2 is the first step in LP activation, and part of a positive feedback loop leading to sustained AP activation, with inflammation and concurrent activation of the coagulation cascade (33,34). Although documented experimentally for SARS-CoV, this binding is speculative in terms of SARS-CoV-2, as certain sites on its glycoprotein spikes are mutated compared to SARS-CoV (35). However, glycosylation sites for high-mannose structures with the potential to similarly engage MBL, and thus activate MASP2, have been identified for SARS-CoV-2 (35). Our data showing co-localization of products linked to activation of the AP (C5b-9) and LP (C4d) with SARS-CoV-2 spike glycoproteins are consistent with this hypothesis.

There may also be pathways apart from virus spike engagement by which LP and AP are activated. First, MBL and ficolins bind to pathogen-associated molecular patterns present on injured cells, enabling complex formation with MASP2 (36). In addition, all three ARDS-linked coronaviruses use ACE2 as an entry point to cells (6). Angiotensin I and angiotensin II have been associated with inflammation, oxidative stress, and fibrosis, and ACE2 is involved in their deactivation (37). If overwhelming coronavirus infection, with binding to ACE2 on epithelial targets not only in the lung but in other tissues expressing these proteins, including the kidney, intestines, and brain, were to interfere with ACE2 activity, the resulting increases in angiotensin II could lead to reactive oxygen species formation and interference with anti-oxidant and vasodilatory signals such as NOX2 and eNOS, with further complement activation. This has been demonstrated in a rat model of angiotensin II over-expression linked to other disorders (38). The potential loss of auto-vasoconstriction and regulation of lung blood flow through injured vascular segments would also lead to increased shunting and severe hypoxemia. Fig. 10 summarizes the potential mechanisms of SARS-CoV2 associated complement activation, and its possible interaction with coagulation pathways.

Given these data, use of agents that block LP activation at MBL recognition domains, such as narsoplimab (OMS721), a humanized monoclonal antibody against MASP-2 which recently received Breakthrough Therapy Designation for hematopoietic stem cell transplant-linked thrombotic microangiopathies (39), or eculizumab, a humanized anti-C5 monoclonal antibody FDA-approved for aHUS, might be considered on a case-by-case basis in severe COVID-19. Investigating critical biomarkers consistent with complement-mediated microvascular injury and thrombosis in COVID-19 patients would be important. A panel to study might include: d-dimers; factor VIII, fibrinogen, and other coagulation factors; antiphospholipid antibodies; C-reactive protein; pro-inflammatory cytokines, particularly IL-1 and IL-6; circulating complement proteins including C3, C4, C5b-9, and Bb (the latter remaining in circulation longer than other components, as a marker of AP activation); and tissue biopsy, the skin being most readily accessible. This could enable establishment of criteria for clinical trials with ant-complement and/or anticoagulants, and perhaps open the possibility for earlier intervention than at the end-stages of severe COVID-19.

References

1. Zhu N, Zhang D, Wang W, et al. A novel coronavirus from patients with pneumonia in China. 2019; *N Engl J Med*. 2020. doi:10.1056/NEJMoa2001017

2. Cucinotta D, Vanelli M. WHO Declares COVID-19 a Pandemic. *Acta Biomed*. 2020. doi:10.23750/abm.v91i1.93973.

3. cdc.gov/coronavirus/2019.ncov

4. Wang D, Hu B, Hu C, et al. Clinical characteristics of 138 hospitalized patients with 2019 novel coronavirus-infected pneumonia in Wuhan, China. JAMA.2020.doi:1585.

5. Tang N, Li D, Wang X, Sun Z. Abnormal coagulation parameters are associated with poor prognosis in patients with novel coronavirus pneumonia. J Thromb Haemost 2020.doi:10.1111/jth.14768.

6. Phan T. Novel coronavirus: From discovery to clinical diagnostics. Infect Genet Evol. 2020 Apr;79:104211. doi: 10.1016/j.meegid.2020.104211.

7.Gralinski LE, Sheahan TP, Morrison TE, et al. Complement activation contributes to severe acute respiratory syndrome coronavirus pathogenesis. mBio. 2018 Oct 9;9(5).

8. Xu Z, Shi L, Wang Y, et al. Pathologic findings of COVID-19 associated with acute respiratory distress syndrome. Lancet Respiratory Med 2020;8:420-422.

9. Zhang H, Zhou P, Wei Y, et al. Histopathologic changes and SARS-Cov-2 immunostaining in the lung of a patient with COVID-19. Ann Intern Med 2020; in press.

10. Zhou F, Yu T, Du R, et al. Clinical course and risk factors for mortality of adult inpatients with COVID-19 in Wuhan, China: a retrospective cohort study. Lancet 2020;395:1054-62.

11. Gattinoni L, Coppola S, Cressoni M, Busana M, Chiumello D. Covid-19 Does Not Lead to a "Typical" Acute Respiratory Distress Syndrome. *Am J Respir Crit Care Med*. March 2020. doi:10.1164/rccm.202003-0817LE

12. Magro CM, Poe JC, Kim C, et al. Degos disease: a C5b-9/interferon-α-mediated endotheliopathy syndrome. Am J Clin Pathol. 2011;135(4):599-610.

13. Magro CM, Momtahen S, Mulvey JJ, Yassin AH, Kaplan RB, Laurence JC. 2015. The role of the skin biopsy in the diagnosis of atypical hemolytic uremic syndrome. Am J Dermatopathol 37:349-359.

14. Magro CM, Pope Harman A, Klinger D, et al. Use of C4d as a diagnostic adjunct in lung allograft biopsies. Am J Transplant 2003;3:1143-1154.

15. Magro CM, Deng A, Pope-Harman A, et al. Humorally mediated posttransplantation septal capillary injury syndrome as a common form of pulmonary allograft rejection: a hypothesis. Transplantation 2002;74:1273-1280

16. Yao XH, Li TY, He ZC, et al. [A pathological report of three COVID-19 cases by minimally invasive autopsies]. *Zhonghua bing li xue za zhi = Chinese J Pathol*. 2020. doi:10.3760/cma.j.cn112151-20200312-00193

17. Chaturvedi S, Braunstein EM, Yuan X, et al. Complement activity and complement regulatory gene mutations are associated with thrombosis in APS and CAPS. *Blood*. 2020. doi:10.1182/blood.2019003863

18. Magro CM, Poe JC, Kim C, et al. Degos disease: A C5b-9/interferon-α-mediated endotheliopathy syndrome. *Am J Clin Pathol*. 2011. doi:10.1309/AJCP66QIMFARLZKI

19. Ruffatti A, Calligaro A, Lacognata CS, et al. Insights into the pathogenesis of catastrophic antiphospholipid syndrome. A case report of relapsing catastrophic antiphospholipid syndrome and review of the literature on ischemic colitis. *Clin Rheumatol*. 2019. doi:10.1007/s10067-019-04888-5

20. Manrique-Caballero CL, Peerapornratana S, Formeck C, Del Rio-Pertuz G, Gomez Danies H, Kellum JA. Typical and Atypical Hemolytic Uremic Syndrome in the Critically Ill. Crit Care Clin 2020; doi:10.1016/j.ccc.2019.11.004

21. Fremeaux-Bacchi V, Fakhouri F, Garnier A, et al. Genetics and outcome of atypical hemolytic uremic syndrome: a nationwide French series comparing children and adults. Clin J Am Soc Nephrol, 2013;8:554-562.

22. Magro CM, Wang X, Garrett-Bakelman F, Laurence J, Shapiro LS, Desancho MT. The effects of Eculizumab on the pathology of malignant atrophic papulosis. Orphanet J Rare Dis; 2013; doi:10.1186/1750-1172-8-185

23. Perera TB, Murphy-Lavoie HM. *Purpura Fulminans*. StatPearls Publishing; 2020. http://www.ncbi.nlm.nih.gov/pubmed/30422460. Accessed March 28, 2020.

24. Rits K, Doumas M, Mastellos D, et al. Anovel C5a receptor-tissue factor cross-talk in neutrophils links innate immunity to coagulation pathways. J Immunol 2006;177:4794-4802.

25. Yen Y-T, Liao F, Hsiao C-H, Kao C-L, Chen Y-C, Wu-Hsieh BA. Modeling the early events of severe acute respiratory syndrome coronavirus infection in vitro. J Virol 2006;80:2684-2693.

26. Fan BE, Chong VCL, Chan SSW, et al. Hematologic parameters in patients with COVID-19 infection. Am J Hematol 2020;doi:10.1002/ajh.25774.

27. Bhatraju PK, Ghassemieh BJ, Nichols M, et al. Covid-19 in critically ill patients in the Seattle region--case series. N Engl J Med 2020;doi:10.1056/NEJMoa2004500.

28. Wysong A, Venkatesan P. An approach to the patient with retiform purpura. Dermatologic Ther 2011;24:151-172.

29. Laurence J, Haller H, Mannucci PM, Nangaku M, Praga M. de Cordoba SR. Atypical hemolytic uremic syndrome (aHUS): essential aspects of an accurate diagnosis. Clin Adv Hematol Oncol 2016;14(11S1):1-15.

30. Prufer F, Scheiring J, Sautter S, et al. Terminal complement complex (C5b-9) in children with recurrent hemolytic uremic syndrome. Sem Thromb Hemost 2006;32:121-7.

31. Chaturvedi S, Braunstein EM, Yuan X, et al. Complement activity and complement regulatory gene mutations are associated with thrombosis in APS and CAPS. Blood 2020;135:239-251.

32. Zhou Y, Lu K, Pfefferle S, et al. A single asparagine-linked glycosylation site of the severe acute respiratory syndrome coronavirus spike glycoprotein facilitates inhibition by mannose-binding lectin through multiple mechanisms. J Virol 2010;84:8753-8764.

33. Beltrame MH, Catarino SJ, Goeldner I, et al. The lectin pathway of complement and rheumatic heart disease. Front Ped 2015;2(148):1-14.

34. Krarup A, Wallis R, Presanis JS, Gal P, Sim RB. Simultaneous activation of complement and coagulation by MBL-associated serine protease 2. PLoS One 2007;7:e623.

35. Walls AC, Park Y-J, Tortorici MA, Wall A, McGuire AT, Veesler D. Structure, function, and antigenicity of the SARS-CoV-2 spike glycoprotein. Cell 2020; doi:10.1016/j.cell.2020.02.058

36. Dodo J, Kocsis A, Gal P. Be on target: strategies of targeting alternative and lectin pathway components in complement-mediated diseases. Front Immunol 2018;9(1851):1-22.

37. Srivastava P, Badhwar S, Chandran DS, Jaryal AK, Jyotsna VP, Deepak KK. Imbalance between Angiotensin II - Angiotensin (1-7) system is associated with vascular endothelial

dysfunction and inflammation in type 2 diabetes with newly diagnosed hypertension. Diabetes Metab Syndr 2019;13:2061-2068.

38. Shagdarsuren E, Wellner M, Braesen JH, et al. Complement activation in angiotensin II-induced organ damage. Circ Res 2005;97:716-724.

39. Rambaldi A, Khaled S, Smith M, et al. Improved survival following OMS721 treatment of hematopoietic stem cell transplant-associated thrombotic microangiopathy (HCT-TMA). Eur Hematol Assoc, Stockholm, Sweden, June 14-17, 2018, Abst PF724.

Acknowledgments

The authors are aware of the journal's authorship statement and only Dr. Laurence has a potential conflict of interest. He has received an unrestricted educational grant and consulting fees from Omeros, Inc. He is also Senior Scientist for Programs at amfAR, The Foundation for AIDS Research, with funding from the Angelo Donghia Foundation.

The expert technical assistance of Bing He, Weill Cornell Medicine, Department of Pathology and Laboratory Medicine, Translational Research Program, is gratefully acknowledged.

Figure Legends

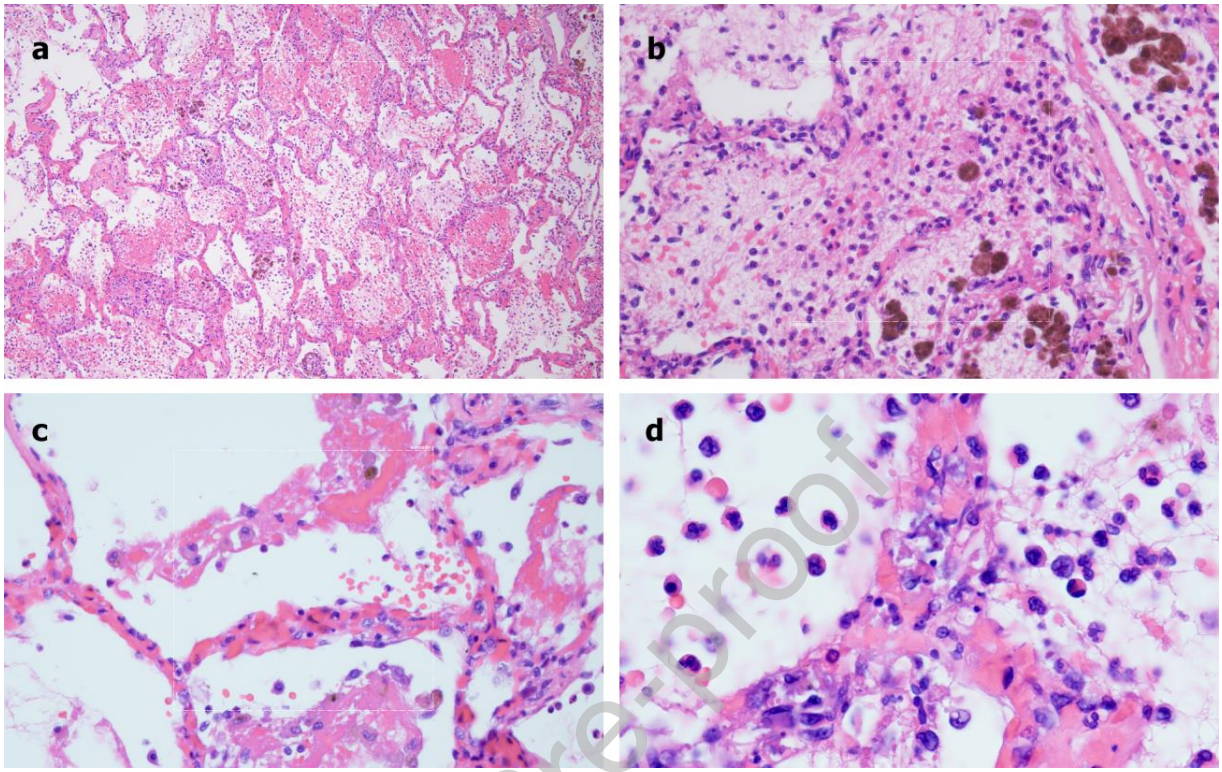

Figure 1. Microscopic features of pulmonary autopsy samples from Case 1. A: Significant fibrin deposition within the inter-alveolar septa and alveolar spaces, accompanied by marked hemorrhage and hemosiderin deposition. (Hematoxylin and eosin stain, 200x.). B: Prominent destructive septal capillary injury is apparent, with fibrinoid necrosis of the capillaries accompanied by evidence of vascular compromise, with hemorrhage and fibrin and hemosiderin deposition within alveolar spaces. (Hematoxylin and eosin stain, 400x.) C: Septal capillary injury is characterized by a pauci-inflammatory response. (Hematoxylin and eosin, 1000x). D: Additional features of the septal capillary injury includes an interstitial and intra-alveolar accumulation of neutrophils. (Hematoxylin and eosin, 400x).

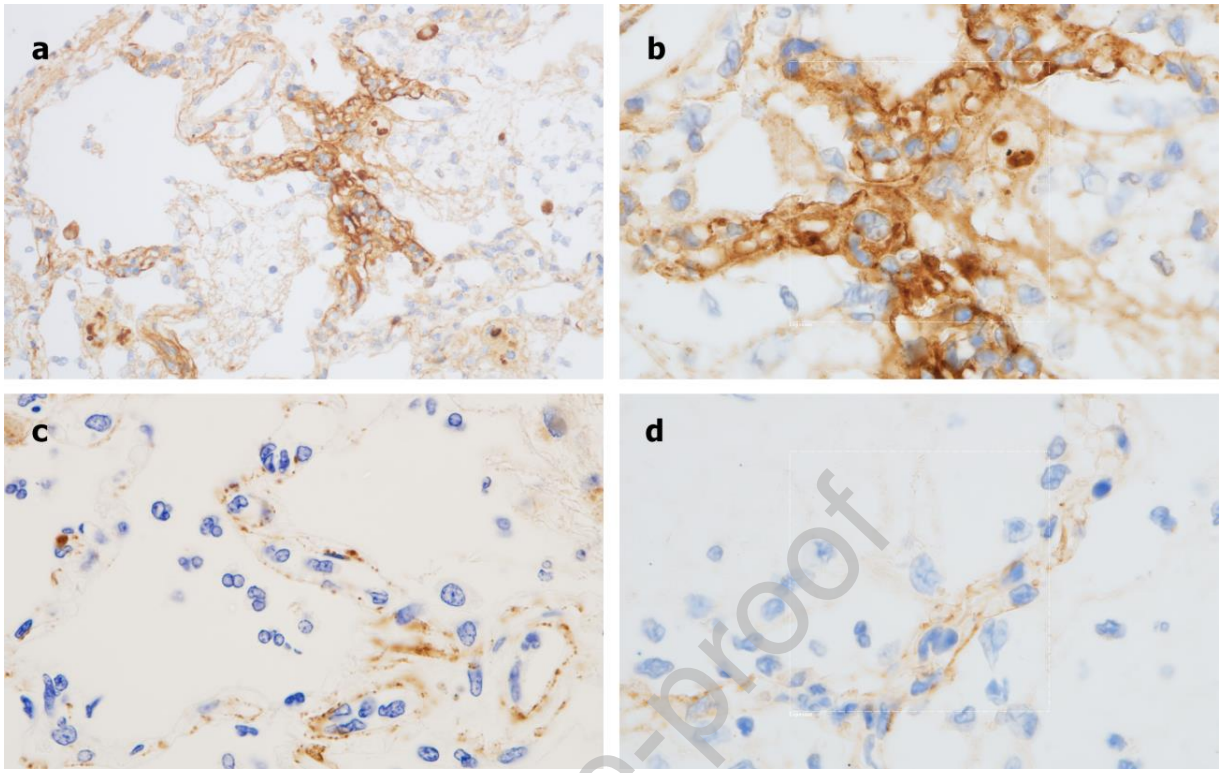

Figure 2. Immunohistochemistry analysis of pulmonary autopsy samples from Case 1. A: Extensive C4d deposition is seen throughout the lung parenchyma, with striking septal capillary localization. (Diaminobenzidene stain, 200x.) B: Higher power magnification documents a clear localization of C4d within septal capillaries. (Diaminobenzidene, 1000x.) C: A similar septal capillary distribution for C5b-9 deposition is observed, although it is less pronounced than that observed for C4d. (Diaminobenzidene, 1000x.) D: A similar septal capillary distribution of C3d staining is observed, although it is also less pronounced than was observed for C4d. (Diaminobenzidene, 1000x.)

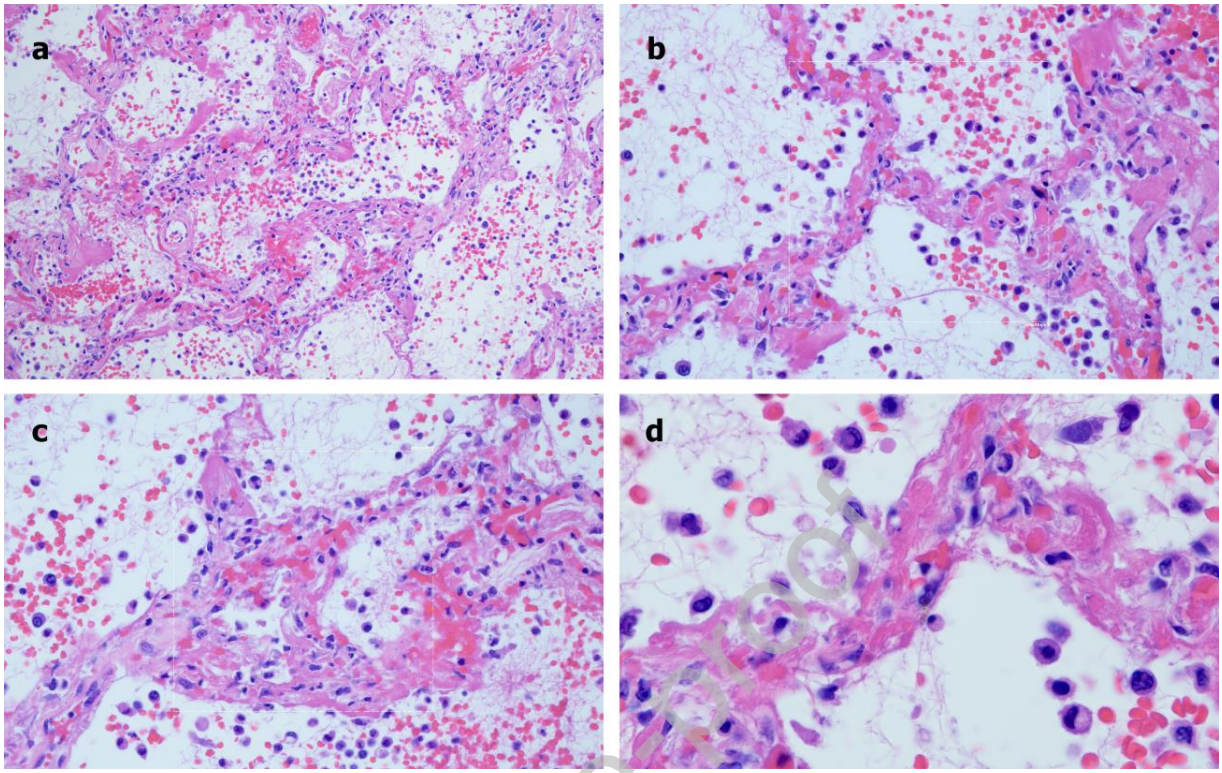

Figure 3. Microscopic features of pulmonary autopsy samples from Case 2. A: Extensive hemorrhagic pneumonitis was seen, with red cell extravasation and fibrin in alveolar spaces and luminal and mural fibrin deposition within septal capillaries. (Hematoxylin and eosin, 200x). B: The septa exhibit a pauci-cellular pattern of capillary injury as evidenced by significant fibrin deposition, with thrombi seen in capillaries. There is red cell extravasation in the alveolar spaces along with collections of neutrophils and monocytes. (Hematoxylin and eosin, 400x). C: There is slight widening of the septa by a few inflammatory cells, predominantly neutrophils. There is evidence of capillary injury characterized by fibrin deposition in the lumens and walls with red cell extravasation within the septa and adjacent alveolar space. Type II pneumocyte hyperplasia and viral cytopathic effects are not discernible. (Hematoxylin and eosin, 400x). D: Higher power examination further illuminates capillary wall disruption accompanied by fibrin deposition and red cell extravasation, with neutrophils in the septa and within the alveolar spaces. (Hematoxylin and eosin, 1000x).

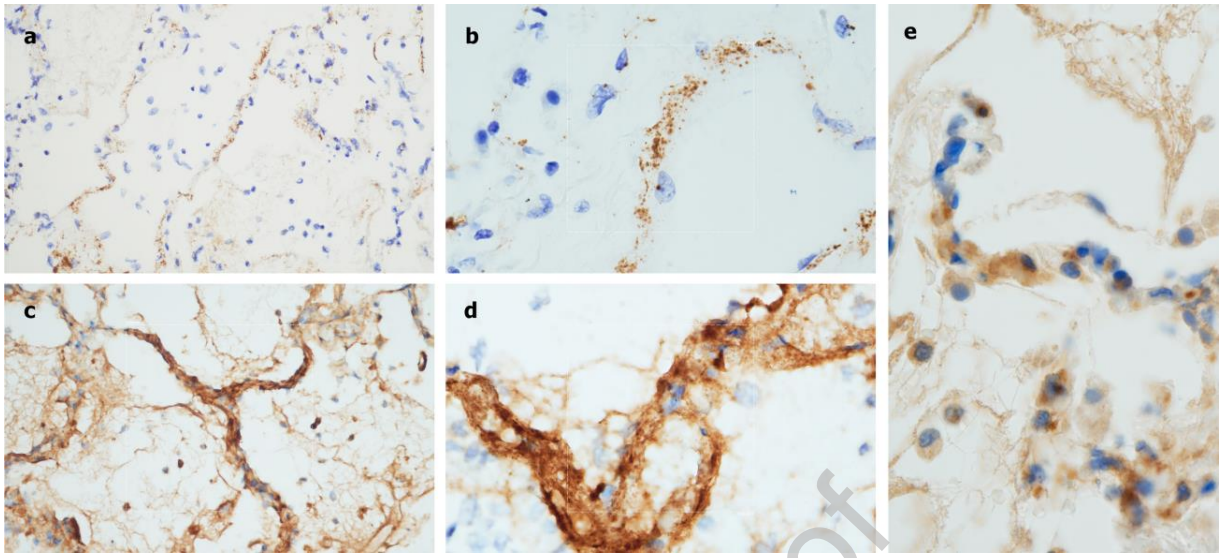

Figure 4. Immunohistochemistry analysis of pulmonary autopsy samples from Case 2. A: There was striking deposition of C5b-9 within the microvasculature of the inter-alveolar septa. (Diaminobenzidene, 200x.) B: Higher power magnification again shows localization of C5b-9 within the septa, including C5b-9 deposits in areas of normal appearing lung, suggestive of systemic complement activation. (Diaminobenizdene, 1000x.) C: C4d deposition was largely localized to the inter-alveolar septa in areas of microvascular injury. (Diaminobenzidene 400x.) D: A higher power image demonstrates the extensive degree of CD4d deposition within the septa. (Diaminobenzidene, 1000x.) E: MASP2 staining showed granular and punctate deposits localized to the inter-alveolar septa.

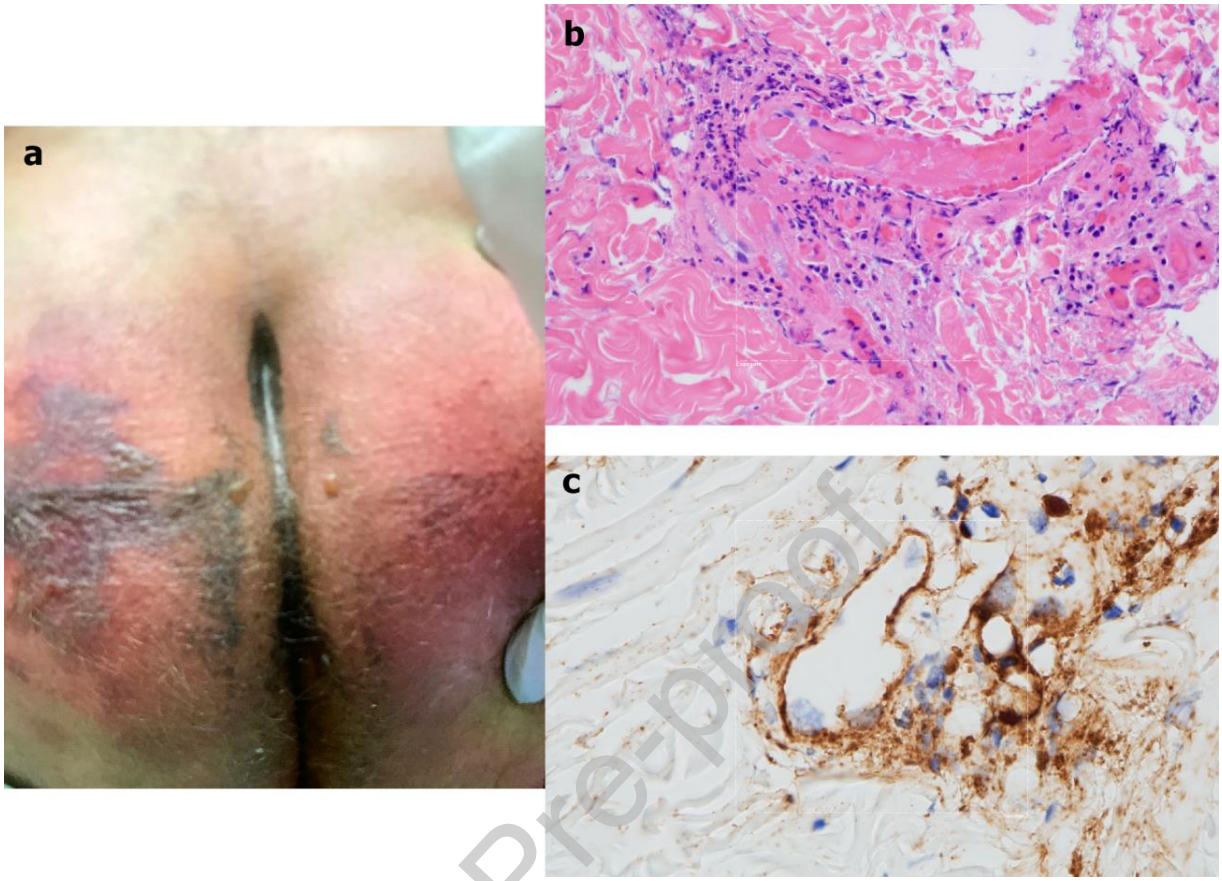

Figure 5. Clinical, microscopic, and immunhohistochemical analyses of Case 3. A: Skin biopsy showed an extensive pattern of pauci-inflammatory vascular thrombosis with endothelial cell injury. (Hematoxylin and eosin, 400x.) B: Prominent deposits of C5b-9 are seen within the microvasculature. (Diaminobenzidene, 400x). C: Striking retiform purpura with surrounding inflammation was noted on the buttocks.

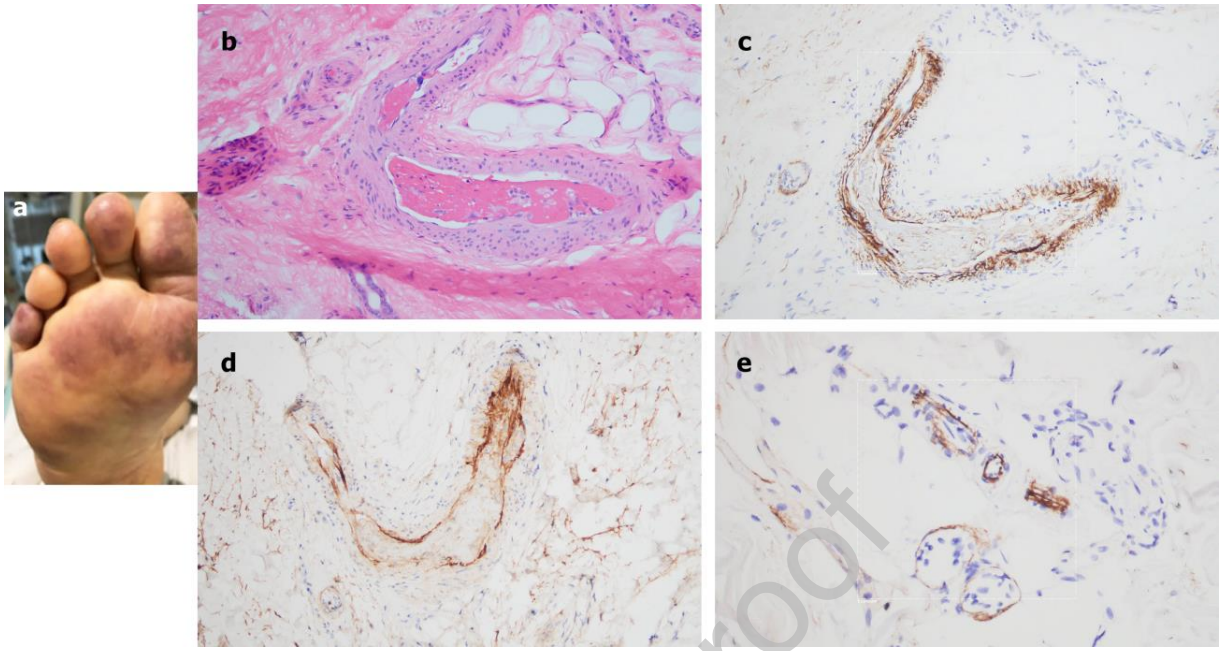

Figure 6. Clinical, microscopic, and immunhohistochemical analyses of Case 4. A: Prominent livedo rashes on the palmar and plantar aspects of the hands and feet, respectively, were noted. B: Skin biopsy demonstrated an occlusive arterial thrombus within deeper dermis. (Hematoxylin and eosin, 200x.) C: Extensive endothelial and subendothelial deposits of C5b-9 are observed within the thrombosed artery. (Diaminobenzidene, 400x.) D: A similar striking pattern of endothelial and subendothelial C4d deposition is noted within the artery. (Diaminobenzidene, 400x.) E: A biopsy of normal-appearing deltoid skin showing conspicuous microvascular deposits of C5b-9. (Diaminobenzidene, 400x.)

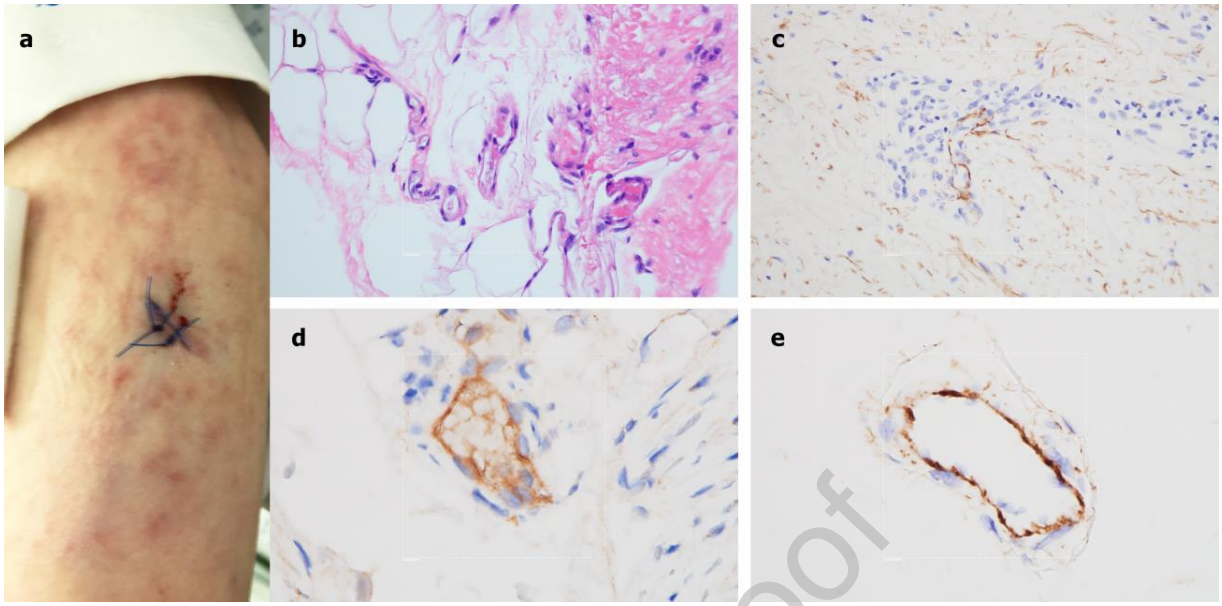

Figure 7. Clinical, microscopic, and immunhohistochemical analyses of Case 5. A: A lacey livedoid rash on the lower extremities was noted. B: A skin biopsy revealed a few deep-seated venules at the dermal-subcuticular interface containing small fibrin thrombi. (Hematoxylin and eosin, 400x.) C: There are significant vascular deposits of C5b-9 within the dermis. (Diaminobenzidene, 400x.) D: Vascular deposits of C4d were also observed within the dermal microvasculature. (Diaminobenzidene, 400x.) E: A biopsy of normal-appearing deltoid skin shows microvascular deposits of C5b-9. (Diaminobenzidene, 400x.)

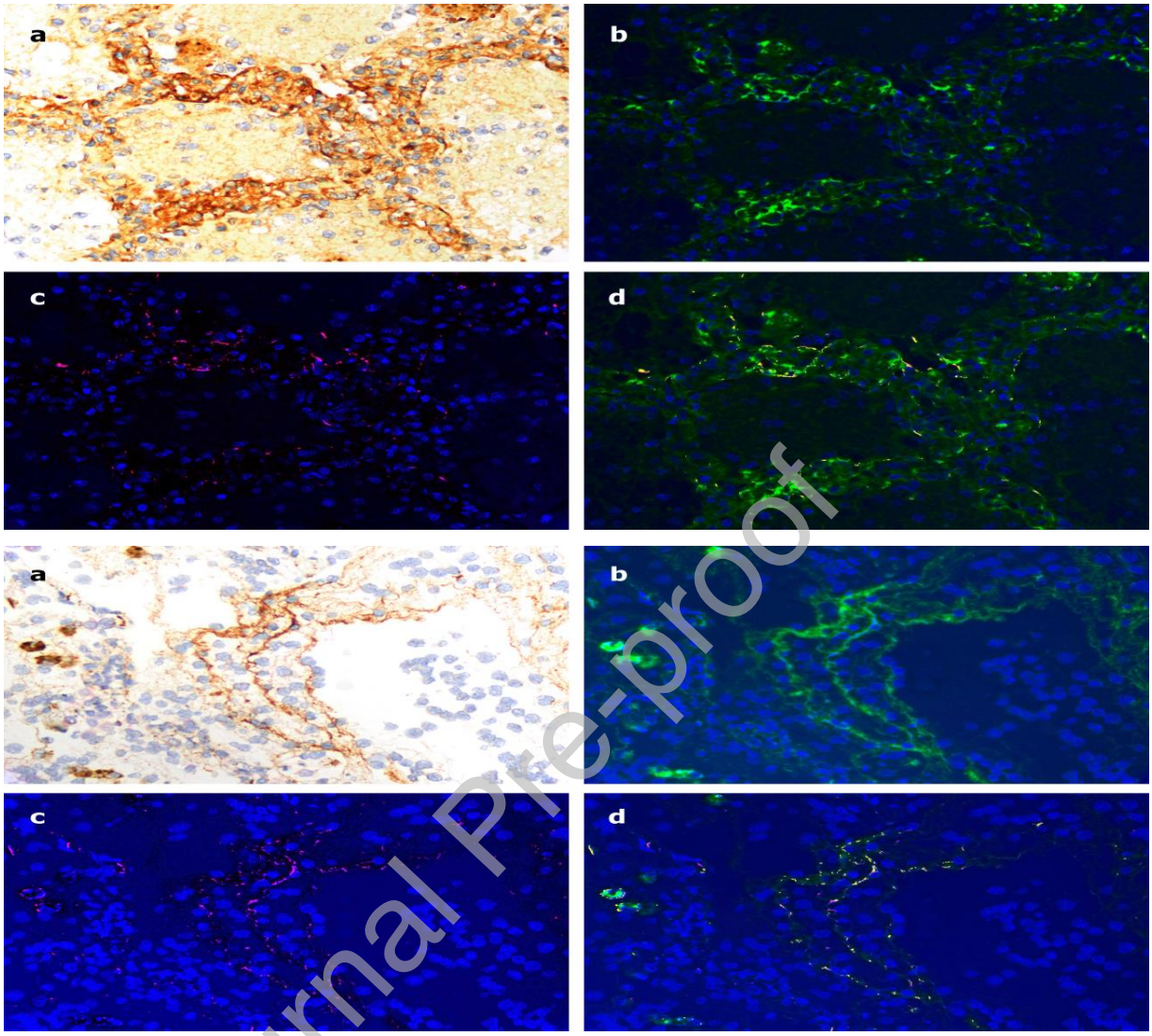

Figure 8. Demonstration of co-localization of complement components with SARS-CoV2 spike glycoprotein in the lung of Case 1. A: Striking deposition of C4d within the inter-alveolar septa of the lung was first demonstrated by DAB staining. Using NUANCE software the C4d image appears green (B) while the SARS-CoV2 spike protein appears red (C). D: A merged image shows a significant degree of C4d and SARS-CoV2 co-localization, as revealed by intense yellow staining. E-H: A similar pattern was observed using an anti-C5b-9 reagent whose image appears green, with a significant degree of C5b-9 and SARS-CoV2 co-localization, as revealed by intense yellow staining.

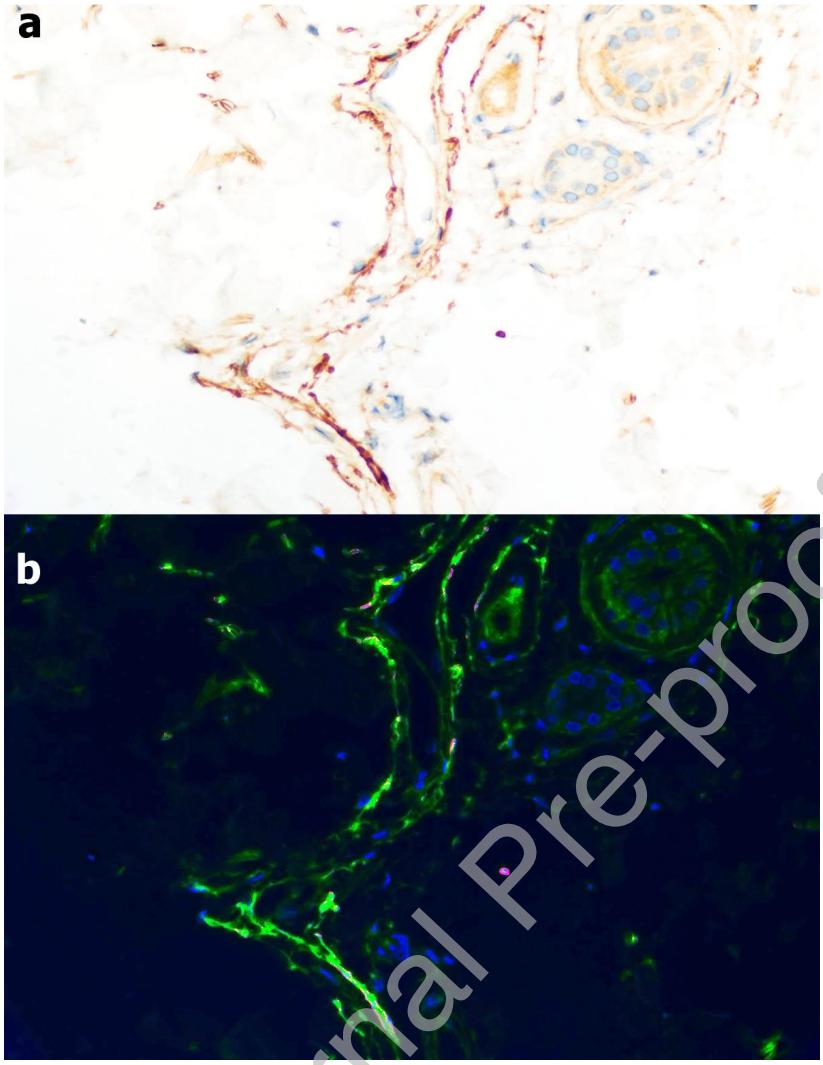

Figure 9. Demonstration of co-localization of C4d and SARS-CoV2 spike glycoprotein in the skin of Case 3. The skin biopsy was stained for C4d showing significant vascular localization (DAB stain). Using NUANCE software C4d is highlighted green while COVID-19 spike protein shows a red staining pattern; a yellow signal is discernible indicative of co-localization of C4d and viral protein within the microvasculature.

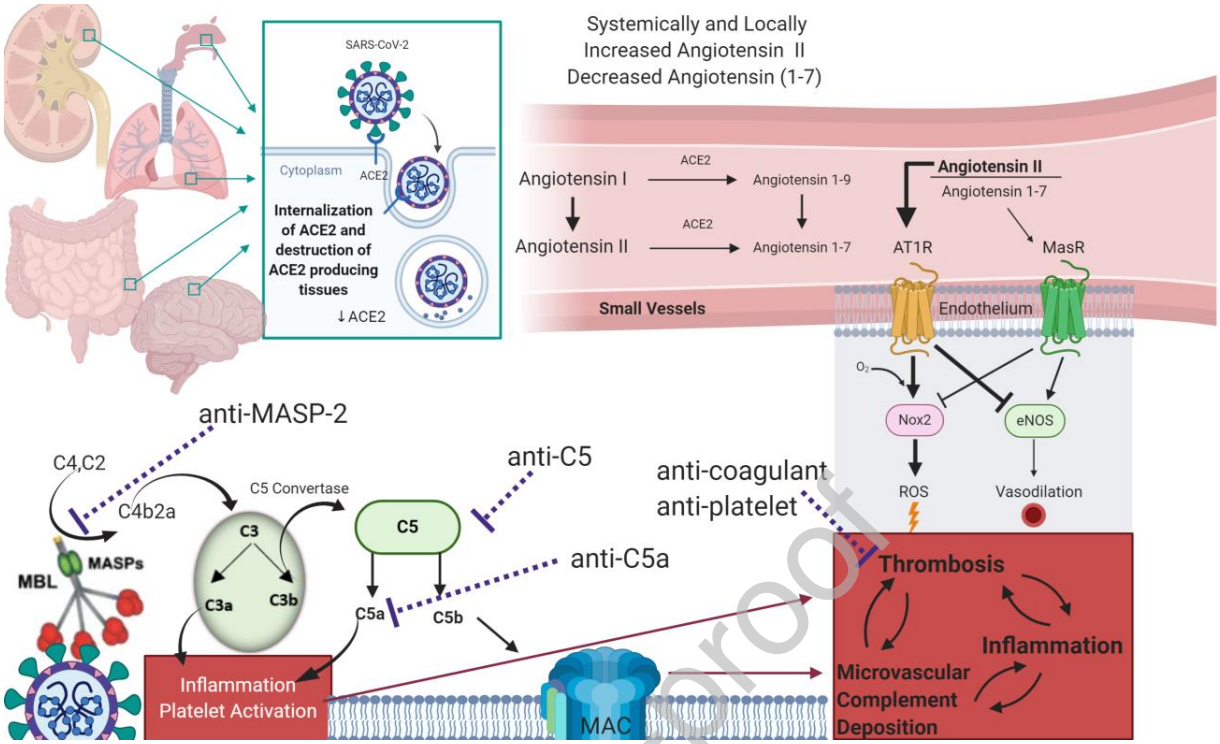

Figure 10: Model for AP and LP complement activation by SARS-CoV2, and its interaction with coagulation cascades.